A General Design Method of Primary Compensation Network for Dynamic WPT System Maintaining Stable Transmission Power

Jinbo Zhao, Tao Cai, Shanxu Duan, *Member, IEEE*, Hao Feng, Changsong Chen, and Xiaoming Zhang

***Abstract*—Dynamic wireless power transmission (DWPT) is considered as a solution to the problems encountered in the development of electrical vehicle (EV), such as range anxiety resulted from battery bottleneck and the difficulty of convenient charging. However, the requirement of DWPT, maintaining almost constant transmission power with constant voltage load in effective movement process, is quite different from Stationary WPT. The power fluctuation is easily brought by the coupling coils over large misalignment in movement. A general design method of primary compensation network from the perspective of DWPT is presented in this paper. Under the premise of ensuring high transmission efficiency and soft switching, a novel T-type compensation network for DWPT is proposed, which maintains a stable output characteristic over a wide misalignment, companied with an inherent current limiting ability under no-load operation. A WPT prototype with a fixed frequency operation based on the T-type compensation network is built. The output power is kept almost stable even though magnetic coupling coefficient varies twice showing the effectiveness of the design method.**

***Index Terms*—Constant transmission power, dynamic wireless power transmission, high-order compensation topology, soft switching, variable magnetic coupling coefficient.**

NOMENCLATURE

α	Ratio between $k_{\max}$ and $k_{\min}$.
β	Proportion between $Z_{\mathrm{cm}1}$ and $Z_{\mathrm{cm}2}$.
$g(x)$	Power transmission factor.
I_{L1}	Current in the primary transmitter coil.
I_{L2}	Current in the secondary receiving coil.
k	Mutual coupling coefficient between power coils.
M	Mutual inductance between power coils.
Q_{L1}	Quality factor of the primary transmitter power coil.
Q_{L2}	Quality factor of the secondary receiving power coil.
Q_{Load}	Secondary quality factor considering the load.
R_d	DC load.
R_L	Equivalent ac load.
U_{d1}	Input dc voltage.
U_{d2}	Output dc voltage.
U_{oc}	Inductive voltage of secondary coil.
ω	Operating angular frequency.
x	Parameter which represents the impact of misalignment.
Z_2	Total impedance of the secondary-side circuit.
$Z_{\mathrm{cm}1}$	Impedance of the first compensation element.
$Z_{\mathrm{cm}2}$	Impedance of the second compensation element.
$Z_{\mathrm{cm}3}$	Impedance of the third compensation element.
Z_{in}	Input impedance of the compensation network.
Z_{L1}	Impedance of primary transmitter coil.
Z_{L2}	Impedance of secondary receiving coil.
Z_r	Reflected impedance of the secondary side.
γ_1	First compensation coefficient.
κ	Second compensation coefficient.
δ	Lateral misalignment percentage.

Manuscript received June 08, 2015; revised November 27, 2015; accepted December 28, 2015. Date of publication January 08, 2016; date of current version July 08, 2016. This work was supported in part by the Funds for International Cooperation and Exchange of the National Natural Science Foundation of China under Grant 51361130150. Recommended for publication by Associate Editor J. Acero.

The authors are with the State Key Laboratory of Advanced Electromagnetic Engineering and Technology, School of Electrical and Electronic Engineering, Huazhong University of Science and Technology, Wuhan 430074, China (e-mail: zhaojinbo@hust.edu.cn; caitao@hust.edu.cn; duanshanxu@hust.edu.cn; fhdtc2008@hust.edu.cn; ccsfm@163.com; ming1006@126.com.cn).

Color versions of one or more of the figures in this paper are available online at http://ieeexplore.ieee.org.

Digital Object Identifier 10.1109/TPEL.2016.2516023

I. INTRODUCTION

In recent years, wireless power transmission (WPT) technology has made rapid development, especially the magnetic coupling WPT technology, which transfers energy through high-frequency magnetic field coupling between transmitter and receiver coils. Magnetic coupling WPT technology has been successfully applied in low-power portable electronic devices [1], [2] such as mobile phones, pacemakers, etc. Another important application of magnetic coupling WPT is to charge electric vehicles (EVs) without contact [3]–[5]. Along with further increase of the transmission power and efficiency, stationary wireless charging is likely to replace the traditional conductive charging in the near future. Meanwhile, EVs are not yet widely accepted by consumers because of the range anxiety suffering from battery bottleneck and the difficulty of convenient charging. As a result, the dynamic wireless power transmission (DWPT) solution [5] is reconsidered. As early as in the 1970s, the proof-of-concept program of roadway inductively powered EV was actually implemented at the University of California, Berkeley, CA, USA [6], but without success due to the limitation of power electronics technology at that time. A general schematic of DWPT is shown in Fig. 1. The moving EV with a receiver coil under its chassis uninterruptedly picks up the power through the coupling magnetic field from the primary transmitter coils chain underneath the powered roadway, effectively extending the driving range [7]. The output of receiving circuit is always attached to the battery or the dc bus of EV. Therefore, the load of DWPT can be regarded as approximate constant voltage type during most of the time [8]–[10]. In the dynamic movement, the secondary receiver coil will couple one by one with the primary coils chain. The interaction time between each primary

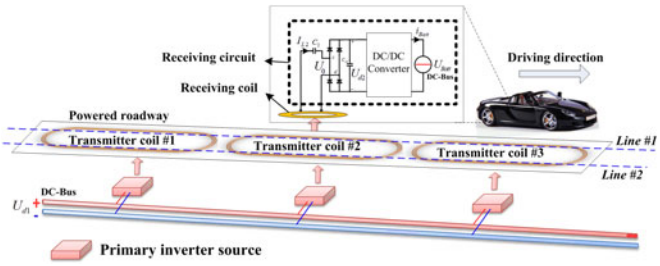

Fig. 1. Schematic of DWPT system.

transmitter coil and the secondary receiver coil is inevitably short. Hence, the communication between primary and secondary sides is not convenient as the stationary WPT. In order to maximize the utilization of the powered roadway in the short interaction time, a DWPT system should pick up the transmission power as much as possible. From the aforementioned dynamic circumstance and the economic benefit, the requirement of the DWPT is quite different from the stationary WPT [11]. The control strategy of the DWPT system generally makes the primary side to operate in a simple fixed-frequency mode, and regulates the receiving power at the secondary side without any communication between both sides [4], [12]. A DWPT system always peruses the maximum rated power transmission in the effective coupling region [13]. Nevertheless, power fluctuation is easily brought by the ineluctable misalignment of receiving coil in movement [7], [13], [14]. For example, EV maybe randomly run along the line #1 or #2, which laterally deviates from the center line of powered roadway as shown in Fig. 1. To increase the utilization of powered charging road, the DWPT system should have internal ability to resist a wide range of misalignment, in other words, maintaining a stable rated transmission power within a certain range of the coupling coefficient k in movement.

In order to increase the tolerance to misalignment, there are two improvements involving magnetic coupler construction and compensation network design. The reconstruction of the magnetic core structure makes the coupling coefficient k remains within a narrow change over a wide range of misalignment. In [15], a flux pipe-type rectangle planer coil with double-sided winding is proposed. This magnetic coupler is similar to solenoid, channeling flux along a maximum length of planer ferrite, thus improving tolerance to horizontal misalignment. A double-D type single-sided flux magnetic coupler compromising the characteristics of the conventional circular coil and flux pipe type coil is introduced in [16], while increasing the vertical and lateral offset range at the same time, doubling the movement range of a single circular coil. Asymmetric coil sets [17], [18] with small-size receiving coil and larger transmitter coil have significantly high lateral tolerance for stationary WPT. In [19], the compact bipolar pads integrate the compensation inductor into the transceiver coils, making the magnetic structure concise. In [20] and [21], an I-shaped core structure for DWPT is constructed. The majority of the magnetic flux constitutes a loop through the before and after interleaving poles, and the area of the receiving coil extends along lateral direction, thus increasing the lateral misalignment tolerance, which is suitable to DWPT.

On the other hand, following the four fundamental compensation networks [22], [23], some high-order compensation topologies are proposed [24]. The *LCL*-type compensation network is the most fit for the DWPT system [25]–[28]. Since it has good characteristics of constant current source, the regulation of the secondary side becomes simple. In [28], the transmission efficiency over the entire coupling region is maintained above 90% due to the dual control strategy on both sides. The hybrid topology on the primary side is proposed in [9], which can switch between two basic compensation networks to satisfy the CV and CC mode for stationary EV charging. In [29], an S/SP prototype compensation topology based on the traditional transformer model is proposed. The operating frequency is set at the load-independent voltage gain points to obtain a good wide load regulation. The transmission efficiency achieves 95% over both wide load range and coupling coefficient range. An SP (CC)-type compensation network which combined the characteristics of both S- and P-type compensation networks is proposed in [30]. The SP-type compensation network possesses relative high misalignment tolerance when a suitable factor K_C is chosen [30]. However, the single design factor K_C is intuitively determined from the transmission power graph which is based on the specific parameters of power coils, resulting in that the K_C is not adjustable. Under the same input source and power coils, the transmission power capacity is the lowest among these types (*LCL*-type, S-type, SP-type). Furthermore, the design method in [30] does not provide the general analytical model versus the coupling coefficient k, resulting in that the best misalignment tolerance is not achieved and the design degree is limited.

From the perspective of smoothing the transmission power fluctuation of DWPT, a general design method and the analytical model of primary compensation network are proposed in this paper. Those fundamental compensation networks based on the single compensation element and high-order compensation networks consisting of multicompensation elements can be all included in the design method. The designed compensation network could smooth the transmission power by automatically adjusting the transmitter coil current according to the variation of the coupling coefficient k as well as the reflected impedance Z_r. Therefore, the effective charging region maintaining stable transmission power is increased without complex control. Meanwhile, it also guarantees the high transmission efficiency and soft switching of primary inverter.

This paper is organized as follows. Section II briefly introduces the basic idea for solving the power fluctuation due to large misalignment. Section III establishes a generalized framework for describing the transmission power of primary compensation network. The transmission power factor $g(x)$ is introduced to indicate the power fluctuation due to the variation of coupling coefficient. The transmission power characteristic versus k with constant voltage load is also obtained. To further ensure the transmission efficiency and soft switching of the primary inverter, the parameters of compensation network are optimized in Section IV. Following the results of the optimization, a T-type compensation network with three freedom degrees is set up. In Section V, the design procedure of the T-type compensation network is given. The proposed compensation network for DWPT is compared with the traditional S-, SP-, and *LCL*-type

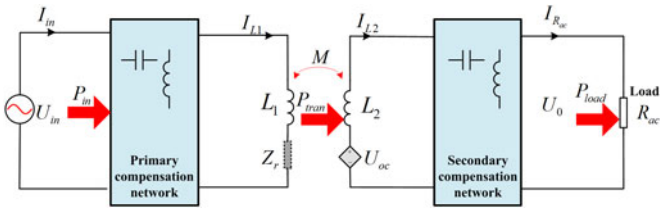

Fig. 2. Block diagram of the WPT system included primary and secondary compensation networks.

compensation networks. Finally, a 400-W DWPT prototype with the T-type compensation network is built. The experimental result shows that the output power can remain stable within the 200% of the coupling coefficient under the constant voltage load or rated resistance load.

II. Basic Idea for Solving Power Fluctuation due to Varied Coupling Coefficient

In DWPT applications, the receiving coil mounted on EV always moves relative to the transmitter coils which are fixed under the powered roadway. Therefore, the coupling coefficient *k* is varied in the dynamic process. The compensation network necessitates good tolerance to high misalignment.

A simplified WPT system is shown in Fig. 2. The power source of fixed frequency $U_{\rm in}$ or $I_{\rm in}$ is commonly generated by the primary inverter, the primary compensation network is inserted between the ac source and transmitter coil. High-frequency current I_{L1} in primary coil generates ac magnetic field coupling with secondary coil. Through the weak magnetic coupling, the power is transmitted across the air gap from the primary side to secondary side. A compensation network is also inserted at the secondary side to compensate the reactive power. Generally at the load side, high-frequency rectifier is required to transfer ac output voltage U_0 into dc output voltage U_{d2} as shown in Fig. 1. According to the number of compensation elements and connecting type, Compensation networks may vary from four fundamental series/parallel types to the high-order types comprised of multiple compensation elements. Without considering the parasitic power loss of the compensation elements, the active power of any part is equal

$$P_{\rm in} = P_{\rm tran} = P_{\rm load} \tag{1}$$

where $P_{\rm in}$ is the active power provided by the primary power source, $P_{\rm tran} = |I_{L1}|^2 \,{\rm Re}(Z_r)$ is the active power transmitted between transceiver coils, $P_{\rm load} = U_0^2/R_{\rm ac}$ is the active power extracted by the load, "Re" represents the real part of impedance. The power capacity of the system depends on the transmission power between transceiver coils. Therefore, we can use $P_{\rm tran}$ as the criteria to analyze the ability of compensation network to regulate the transmission power.

In order to reduce the unnecessary loss of power on the transceiver coils, the secondary compensation network is generally set to the unity power factor pickup mode [31], [32]. Its principle is to ensure that only active power is transferred between transceiver coils. Without loss of generality, it is assumed that the secondary compensation network is of the basic S-type, the secondary impact on the primary side can be equivalent to the reflected impedance as below [33]

$$Z_r = (\omega M)^2/Z_2 = k^2 Q_{\rm load}\,|Z_{L1}| \tag{2}$$

where $Z_{L1} = j\omega L_1$ is the impedance of the transmitter coil, $Z_{L2} = j\omega L_2$ is the impedance of the receiver coil, and $Q_{\rm load} = |Z_{L2}|/R_{\rm ac}$ is the secondary quality factor including the load. The transmission power is expressed as

$$P_{\rm tran} = |I_{L1}|^2\,{\rm Re}(Z_r) = |I_{L1}|^2\,k^2 Q_{\rm load}\,|Z_{L1}|\,. \tag{3}$$

As the well-designed DWPT maintains stable transmission power and the output is approximate constant voltage, the rated charging load can be regarded as approximately constant. It can be seen from (3) that the factors that affect the transmission power are primary current I_{L1} and the coupling coefficient *k*.

The varied *k* due to misalignment does not influence the secondary impedance Z_2, but affects the reflected impedance Z_r, thereby changing the operating status of the primary compensation network as well as the transmission $P_{\rm tran}$. Thus, the primary compensation network is well worth improving to reduce the power fluctuation. When *k* or Z_r changes, the primary compensation network should have the ability to automatically regulate the transmitter coil current I_{L1}, smoothing the fluctuation of $P_{\rm tran}$. Generally, self-regulation ability can be obtained by the basic circuit principles including voltage dividing and current shunting. In the following section, how to design suitable compensation network is discussed.

III. Generalized Framework for Describing Self-Regulation Ability of Compensation Network

To simplify the analysis without loss of generality, some reasonable assumptions and premises are supposed: 1) the primary side operates at fixed frequency during DWPT process. Only the fundamental frequency component is considered because the filtering effect of compensation network [26], [34] makes the currents in transceiver coils nearly sinusoidal. The assumption can be validated by experimental result in Fig. 18(b), (d), Section V; 2) the parasitic loss is omitted in the analysis of the transmission power characteristic of compensation network; 3) for increasing the transfer power and efficiency, the secondary side is set to the unity power factor pickup mode [31], [32]. Only the active power is transferred between transceiver coils; 4) the secondary circuit and the rated load are fixed, only considering the effect of variation of the coupling coefficient *k*.

For the primary current excitation, the first compensation element $Z_{\rm cm1}$ should be parallel with the transmitter coil to automatically adjust the transmission power. However, the current excited compensation network can be transformed into voltage excited one using Thevenin's theorem, as shown in Fig. 3. Therefore, the analysis of voltage excited compensation network is also suitable for the current excited one. Since the voltage excited WPT system is more popular, the following section will focus on voltage excited compensation network.

A. Compensation Network With Multiple Compensation Elements

If the primary ac source is a voltage excitation, there are basically three types of which all compensation elements are involved in automatic regulation of the transmission power. They

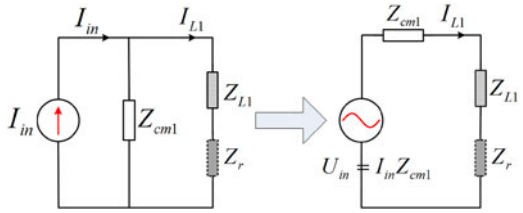

Fig. 3. Thevenin–Norton equivalent transformation between the current and the voltage excited compensation networks.

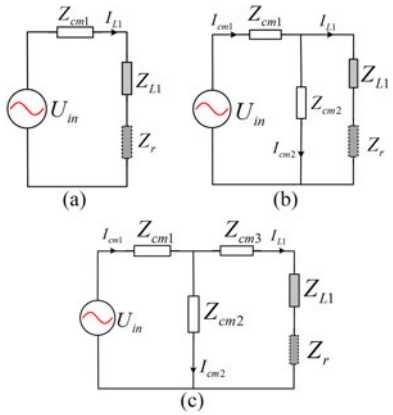

Fig. 4. Voltage excited compensation networks. (a) (S-type) series compensation. (b) (SP-type) series and parallel compensation. (c) (T-type) series, parallel, and series compensation.

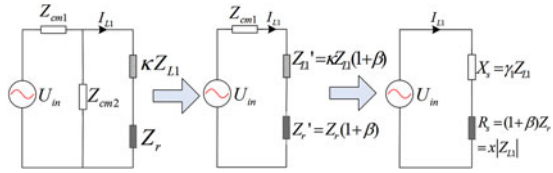

Fig. 5. Equivalent transformation of T-type compensation network maintaining the transmitter coil current I_{L1} unchanged.

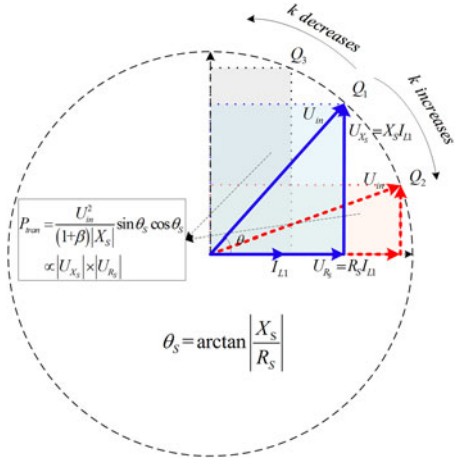

Fig. 6. Phasor diagram showing self-regulation principle of the equivalent series-type compensation network.

are S-type, SP-type, and T-type, as show in Fig. 4. The T-type covering the other two types is more general. The reactance of three compensation elements respectively are $Z_{\rm cm1}$, $Z_{\rm cm2}$, and $Z_{\rm cm3}$, where $Z_{\rm cm1}$ divides the input voltage $U_{\rm in}$, $Z_{\rm cm2}$ shunts the input current $I_{\rm cm1}$, and $Z_{\rm cm3}$ adjusts the reactance of transmitter coil branch.

The input impedance seen by the excitation source can be expressed as

$$Z_{\rm in} = Z_{\rm cm1} + \frac{Z_{\rm cm2}(\kappa Z_{L1} + Z_r)}{(Z_{\rm cm2} + \kappa Z_{L1} + Z_r)} \tag{4}$$

where compensation coefficient $\kappa = (Z_{L1} + Z_{\rm cm3})/Z_{L1}$ shows the compensation degree of the transmitter coil branch. The currents in each branch can be stated as

$$\begin{cases} I_{\rm cm1} = \dfrac{U_{\rm in}}{Z_{\rm in}} \\ I_{L1} = I_{\rm cm1}\dfrac{Z_{\rm cm2}}{Z_{\rm cm2} + \kappa Z_{L1} + Z_r}. \end{cases} \tag{5}$$

Substituting (4) into (5), the current in transmitter coil is

$$I_{L1} = \frac{U_{\rm in}}{Z_{\rm cm1} + (\kappa Z_{L1} + Z_r)(1+\beta)} = \frac{U_{\rm in}}{X_s + R_s} \tag{6}$$

where $\beta = Z_{\rm cm1}/Z_{\rm cm2}$ is the proportion of the first and second compensation elements. As can be seen from (6), the function of adding $Z_{\rm cm2}$ is similar to the impedance transformation, changing the impedance $(\kappa Z_{L1} + Z_r)$ of transmitter coil branch in proportion of real number $(1+\beta)$ as shown in Fig. 5. Noting that the equivalent transformation keeps the transmitter coil current I_{L1} unchanged.

Therefore, the self-regulation principle of T-type compensation network is similar to the equivalent S-type compensation network composed of the reactance X_S and the resistance R_S

$$\begin{cases} X_{\rm S} = Z_{\rm cm1} + \kappa Z_{L1}(1+\beta) = \gamma_1 Z_{L1} \\ R_S = (1+\beta)Z_r = x\,|Z_{L1}| \end{cases} \tag{7}$$

where $\gamma_1 = [Z_{\rm cm1} + \kappa Z_{L1}(1+\beta)]/Z_{L1}$ indicates the compensation degree and power regulation ability of the equivalent S-type compensation network as shown in Fig. 5; $x = R_S/|Z_{L1}| = |1+\beta|k^2 Q_{\rm load}$ represents the relative load which is corresponding to the Z_r in the T-type compensation network, reflecting the impact of the varied coupling coefficient k. The tendency of transmission power versus $x(k)$ can be simply explained in the phasor diagram as shown in Fig. 6. The magnitude of $U_{\rm in}$ keeps the same when the voltage excitation is applied. When the relative load R_S changes due to the varied k, the transmitter coil current I_{L1} is changed accordingly. Since the X_S is constant as long as the compensation network is fixed, the magnitude of I_{L1} is proportional to the voltage U_{X_S}. Therefore, the transmission power is in proportion to the area of rectangle enclosed by the U_{X_S} and U_{R_S}. From the geometric relationship of the phasors, the transmission power is maximum when the phasor $U_{\rm in}$ points at Q_1 where the angle θ_S is 45°. When k decreases or increases from the $k_{\rm set}$ value (corresponding to the point Q_1), the phasor $U_{\rm in}$ moves away from the point Q_1 and the area of rectangle as well as the corresponding transmission power decreases. If the designed compensation network can set the phasor $U_{\rm in}$ at the point Q_1, the transmission power is smooth, although k is fluctuated around the $k_{\rm set}$. The detailed analysis is given as following.

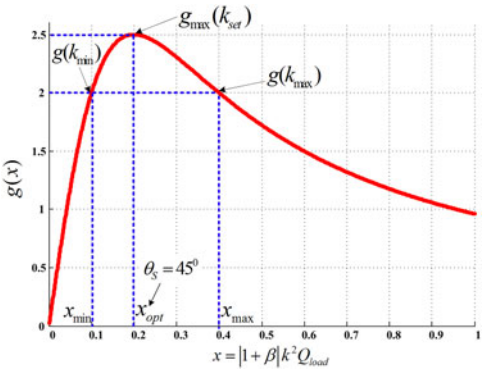

Fig. 7. Power transmission factor $g(x)$ varied with parameter x, setting $\gamma_1 = 0.2$.

Substituting (6) into (3) or from the phasor diagram shown in Fig. 6, the transmission power can be obtained

$$\begin{cases} P_{\text{tran}}(x) = \dfrac{U_{\text{in}}^2}{|1+\beta|\,|X_S|}\sin\theta_S\cos\theta_S = \dfrac{|U_{\text{in}}|^2}{|Z_{L1}|}\dfrac{1}{|1+\beta|}g(\gamma_1,x) \\ g(\gamma_1,x) = \dfrac{1}{\gamma_1}\sin\theta_S\cos\theta_S = \dfrac{1}{\left(\gamma_1^2/x+x\right)} \end{cases} \tag{8}$$

where $\theta_S = \arctan|X_S/R_S|$ is the angle of the phasor U_{in}, and $g(\gamma_1, x)$ is the defined power transmission factor which indicates the relative transmission power capacity. When the parameters of compensation network are set, these compensation coefficients $(\gamma_1, \ldots, \beta)$ are also fixed as real numbers. If $|Z_{\text{cm3}}| \to 0$ or equivalently $\kappa = 1$, the T-type compensation network goes back to SP-type as shown in Fig. 4(b). If $|Z_{\text{cm3}}| \to 0$ and $|Z_{\text{cm2}}| \to$ or equivalently $\kappa = 1$ and $\beta = 0$, the T-type compensation network goes back to S-type as shown in Fig. 4(a). Therefore, the transmission power characteristic of all primary compensation networks can be represented by the power transmission factor $g(\gamma_1, x)$ uniformly. Fortunately, compared with two other compensation networks, the T-type provides three freedom degrees of $(\gamma_1, \kappa, \beta)$ for adjusting the transmission characteristic, which are corresponding to the three compensation elements.

B. Power Fluctuation of Compensation Network Versus Varied x

Providing compensation coefficient $\gamma_1 = 0.2$, power transmission factor $g(\gamma_1, x)$ varied with parameter x is shown in Fig. 7. The $g(x)$ has an extreme point which is determined by the compensation coefficient γ_1. Solving $\partial g(x)/\partial x = 0$, the extreme point is $x_{\text{opt}} = |\gamma_1|$, corresponding to the 45° angle θ_S of phasor U_{in}. The maximum power transmission factor is denoted as

$$\begin{cases} g_{\max}(x_{\text{opt}}) = 1/(2\,|\gamma_1|) \\ x_{\text{opt}} = |\gamma_1|\,. \end{cases} \tag{9}$$

Obviously, the variation of $g(x)$ in the vicinity of x_{opt} is relatively flat. The same transmission power characteristic, reducing the power fluctuation, has been shown in the phasor diagram of Fig. 6. To smooth the transmission power within an ideal range of k, appropriate compensation coefficients $(\gamma_1, \kappa, \beta)$ should be chosen so that corresponding parameter x is in the vicinity of the extreme point $x_{\text{opt}} = |\gamma_1|$. Assuming that the effective range of k is $(k_{\min}, k_{\max})$, where $k_{\max} = \alpha k_{\min}$, and the corresponding range of x is $(x_{\min}, x_{\max})$, where $x_{\max} = \alpha^2 x_{\min}$. For example, the typical range of k is (0.15, 0.3), we can set $\alpha = 2$. There are two cases in which the power fluctuation may be minimal.

1) When $|\gamma_1| < x_{\min}$: In this case, the maximum transmission power is obtained at $x_{\min}(k_{\min})$ point, and the minimum transmission power occurs at $x_{\max}(k_{\max})$ point. As a result, the relative power fluctuation in the effective range of k is

$$\begin{aligned} \Delta_g &= \frac{g(x_{\min}) - g(x_{\max})}{[g(x_{\min}) + g(x_{\max})]/2} \\ &= 2\frac{(\alpha^2-1)}{(\alpha^2+1)}\left[1 - \frac{2}{\alpha^2\left(x_{\min}/\gamma_1\right)^2+1}\right]. \end{aligned} \tag{10}$$

As can be seen in (10), Δ_g is decreasing when γ_1 becomes close to $x_{\min}$. The minimal $\Delta_g = 2(\alpha^2-1)^2/(\alpha^2+1)^2 = 72\%$ when $\gamma_1 = x_{\min}$.

2) When $|\gamma_1| \in (x_{\min}, x_{\max})$: In this case, the maximum transmission power is obtained at extreme point $x_{\text{opt}} = |\gamma_1|$. When the minimum transmission power happens simultaneously at $x_{\min}$ and $x_{\max}$ points, Δ_g becomes minimal. Setting (10) to zero, the relationship of γ_1 and $(x_{\min}, x_{\max})$ can be obtained

$$\begin{cases} x_{\min} = \gamma_1/\alpha \\ k_{\min} = k_{\text{set}}/\sqrt{\alpha} \end{cases} \tag{11}$$

where k_{set} is the rated coupling coefficient corresponding to the extreme point $x_{\text{opt}} = |\gamma_1|$. As a result, the relative power fluctuation is

$$\Delta_g = \frac{g(k_{\text{set}}) - g(k_{\min})}{[g(k_{\text{set}}) - g(k_{\min})]/2} = 2\frac{(\alpha+1/\alpha)-2}{[2+(\alpha+1/\alpha)]}. \tag{12}$$

As can be seen in (12), the minimal Δ_g is only determined by the ratio α, having nothing to do with $x_{\min}$. When the ratio of range k is $\alpha = 2$, the corresponding minimal relative power fluctuation is always $\Delta_g = 22.2\%$. Comparing the above two cases, it can be concluded that $\gamma_1 = x_{\min}/\alpha$ or $k_{\text{set}} = \sqrt{\alpha}k_{\min}$ guarantees the minimal power fluctuation.

C. Power Transmission Characteristic of Compensation Network With Constant Voltage Load

As can be seen in Figs. 1and 9(a), the output of receiving circuit is always attached to voltage-type load, such as dc bus of EV. Therefore, the load of DWPT can be regarded as approximate constant voltage source. To maximize the utilization of powered road, the charging mode of the DWPT system prefers approximate constant power mode. If the compensation network can maintain approximate constant power by itself under the given transmission voltage gain, the proposed compensation network will reduce the reliance on the fast control of the added dc–dc converter at the secondary side. Combining (1) and (8), the voltage gain can be expressed as

$$G_V = \frac{U_{d2}}{U_{d1}} = \frac{U_0}{U_{\text{in}}} = \sqrt{\left|\frac{Z_{L2}}{Z_{L1}}\right|\frac{1}{\frac{\gamma_1^2}{k^2} + \left(|1+\beta|\,Q_{\text{load}}\right)^2 k^2}}. \tag{13}$$

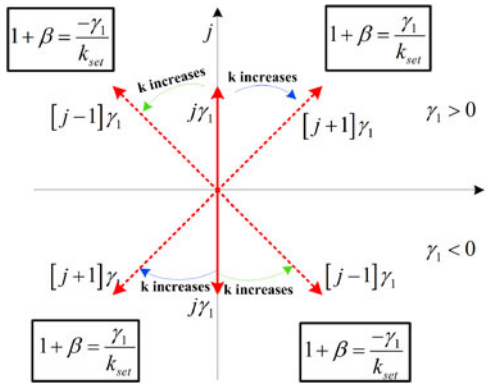

Fig. 8. Phase angle of $Z_{\mathrm{cm}1L1'Zr'}$ varied with k, there are four cases, respectively, distributed in four quadrants.

From (13), the Q_{load} which satisfies the given G_V is obtained

$$Q_{\mathrm{load}}=\frac{R_{\mathrm{ac}}}{|Z_{L2}|}=\frac{\left(2\sqrt{2}/\pi\right)^2 R_{d2}}{|Z_{L2}|}. \tag{14}$$

As a result, the corresponding dc load resistance R_{d2} and the charging dc current I_{d2} are also determined by the settled voltage gain G_V. Substituting (14) into (13), we can get the equivalent dc load resistance R_{d2} and the output dc current I_{d2}

$$I_{d2}=\frac{U_{d2}}{R_{d2}}=\frac{\left(2\sqrt{2}/\pi\right)^2 U_{d2}}{|1+\beta|\,Z_{L2}}\sqrt{\frac{1}{k^2}\left(\left|\frac{Z_{L2}}{Z_{L1}}\right|\frac{1}{G_V^2}-\frac{\gamma_1^2}{k^2}\right)}. \tag{15}$$

The transmission power characteristic with constant voltage load will be further discussed with designed compensation network in Section V. It will show that the transmission power with suitable constant output voltage can keep stable when the compensation network is designed appropriately according to the rated load.

IV. Design Consideration for Compensation Network Parameter

Compensation network parameters should be optimized at the selected coupling coefficient k_{set} so that transmission power keeps stable in the vicinity of k_{set}, simultaneously promising maximum transmission power and efficiency. When k varies from the maximum $k_{\max}$ to zero in the movement process, the inverter bridge needs to operate at soft-switching state, and no-load limiting ability should be ensured for the primary-side safety.

A. Efficiency Consideration

Compensation element commonly use resonant capacitive and inductive elements, and their Q value can be as high as several hundreds. The power loss of primary and secondary network is mainly on the loss of power coils. Therefore, the derivation of the transmission efficiency based on the basic S-type compensation network can be approximately applied to high-order compensation network. Assuming the Q_L of transceiver coils are the same, the optimal Q_{load} at the given coupling coefficient

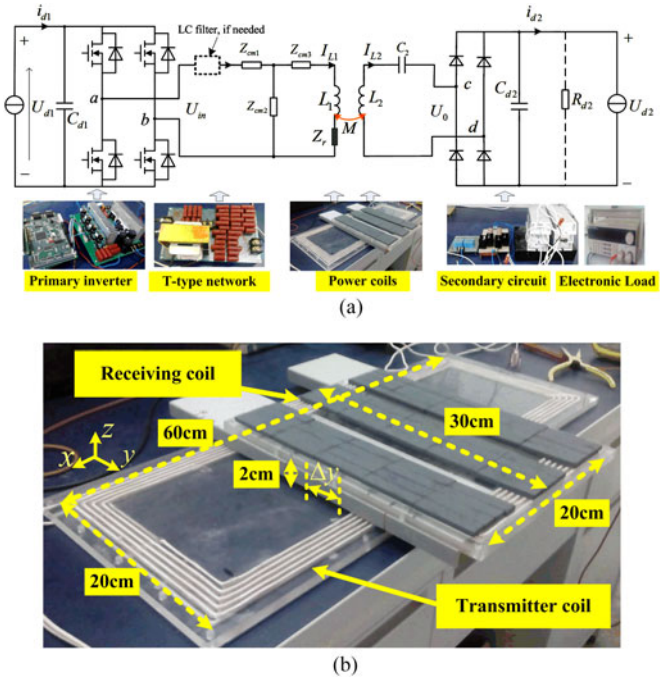

Fig. 9 WPT prototype based on T-type compensation network. (a) Schematic of WPT system and the corresponding experimental setup. (b) Experimental power coils.

k_{set} is [3], [4], [33]

$$Q_{\mathrm{load}}^{\mathrm{opt}}=1/k_{\mathrm{set}}. \tag{16}$$

Substituting (16) into x expression

$$x=(1+\beta)k^2Q_{\mathrm{load}}^{\mathrm{opt}}=(1+\beta)k^2/k_{\mathrm{set}}. \tag{17}$$

In fact, if the actual load is not optimal value, the dc–dc converter for impedance matching is usually added at the secondary side [35], [36]. The load matching problem is out of this paper's scope. So only the case at the optimal load and the settled output voltage is analyzed.

B. Transmission Power Consideration

From the characteristic of transmission factor $g(\gamma_1,x)$, setting $|\gamma_1|=x_{\mathrm{set}}$ ensure that the power fluctuation in the vicinity of the k_{set} minimum. According to efficiency optimization result shown in (16) and (17), the secondary load quality factor Q_{load} is selected according to the k_{set}, and then the β is also determined

$$|1+\beta|=|\gamma_1|/k_{\mathrm{set}}. \tag{18}$$

The transmission power at k_{set} is analyzed to present the rated transmission power capacity of the WPT system

$$P_{\mathrm{tran}}(k_{\mathrm{set}})=\frac{|U_{\mathrm{in}}|^2}{|Z_{L1}|}\frac{k_{\mathrm{set}}}{2\,|\gamma_1|^2}. \tag{19}$$

Therefore, the compensation coefficient γ_1 is selected according to the required transmission power $P_{\mathrm{tran}}(k_{\mathrm{set}})$

$$|\gamma_1|=\sqrt{k_{\mathrm{set}}\frac{|U_{\mathrm{in}}|^2/|Z_{L1}|}{2P_{\mathrm{tran}}(k_{\mathrm{set}})}}. \tag{20}$$

C. Soft-Switching Consideration

In order to reduce the switching losses of the inverter bridge, the output current i_{cm1} of the inverter bridge must be slightly lagged to the output square-wave voltage u_{ab} to meet ZVS condition. In addition, the inverter bridge output port should not be directly parallel with the compensation capacitor; otherwise, it will have a huge overshoot current at switching time.

Transmission power capacity determines the γ_1 as shown in (20). The optimal transmission efficiency decides Q_{load} according to (16). However, the principle of minimum power fluctuation requires $\gamma_1 = x_{\mathrm{opt}}(k_{\mathrm{set}})$. Thus, ratio factor β, which is already determined by the k_{set} and γ_1 as shown in (18), is not an adjustable coefficient. Fortunately, the T-type compensation network has three degrees of freedom, such as (γ_1, κ, β). Therefore, the last compensation coefficient κ happens to the third design freedom for ZVS condition. The impact of the κ on the phase angle $\theta_{z\mathrm{in}}$ is analyzed below.

According to (4) and (5), the input impedance seen from the excitation source can be restated as

$$Z_{\mathrm{in}} = \frac{(1+\beta)(\kappa Z_{L1} + Z_r) + Z_{\mathrm{cm1}}}{1 + (\kappa Z_{L1} + Z_r)/Z_{\mathrm{cm2}}} = \frac{Z_{\mathrm{cm1}L1'Zr'}}{\zeta} \tag{21}$$

where $Z_{\mathrm{cm1}L1'Zr'}$ is the series impedance Z'_{L1} of the transmitter coil branch after equivalent transformation shown in Fig. 5, and ζ is the ratio between I_{cm1} and I_{L1}

$$\begin{cases} Z_{\mathrm{cm1}L1'Zr'} = (1+\beta)(\kappa Z_{L1} + Z_r) + Z_{\mathrm{cm1}} \\ \qquad\qquad = \left[j \pm \dfrac{k^2}{k_{\mathrm{set}}^2} \right] \gamma_1 |Z_{L1}| \\ \zeta = \left(1 + \frac{\kappa Z_{L1} + Z_r}{Z_{\mathrm{cm2}}}\right) = \left(\dfrac{(\gamma_1 - \kappa) - j\frac{k^2}{k_{\mathrm{set}}^2}(\pm\gamma_1 - k_{\mathrm{set}})}{\gamma_1\left(1 - \pm\frac{\kappa}{k_{\mathrm{set}}}\right)} \right). \end{cases} \tag{22}$$

Since the coefficients (γ_1,β) have already been determined, the impact of κ to $\theta_{z\mathrm{in}}$ is determined by ζ. Note that the real part of ζ does not vary with the coupling coefficient k and only its imaginary part changes with k. It is required that Z_{in} is slightly inductive from $k_{\min}$ to $k_{\max}$. In order to analysis the phase angle $\theta_{z\mathrm{in}}$, the phase angles of $Z_{\mathrm{cm1}L1'Zr'}$ and the ratio $\zeta = I_{\mathrm{in}}/I_{L1}$ are, respectively, discussed in four cases.

First, the phase angle of $Z_{\mathrm{cm1}L1'Zr'}$ is discussed in the cases of $1+\beta = \pm\gamma_1/k_{\mathrm{set}}$.

1) $1+\beta = -\gamma_1/k_{\mathrm{set}}$ When $k = 0 \to k_{\mathrm{set}}$, according to the positive or negative first compensation coefficient γ_1, the trend of $Z_{\mathrm{cm1}L1'Zr'}$ phase angle varies in the counterclockwise direction, respectively, in the second quadrant or the fourth quadrant, as shown in Fig. 8

$$\begin{cases} \gamma_1 > 0, 1+\beta = \dfrac{-\gamma_1}{k_{\mathrm{set}}} < 0: \ \theta_{Z_{\mathrm{cm1}L1'Zr'}} = 90^\circ \to 135^\circ \\ \gamma_1 < 0, 1+\beta = \dfrac{-\gamma_1}{k_{\mathrm{set}}} > 0: \ \theta_{Z_{\mathrm{cm1}L1'Zr'}} = -90^\circ \to -45^\circ \end{cases}.$$

2) $1+\beta = +\gamma_1/k_{\mathrm{set}}$ When $k = 0 \to k_{\mathrm{set}}$, according to the positive or negative first compensation coefficient γ_1, the trend of $Z_{\mathrm{cm1}L1'Zr'}$phase angle changes in the clockwise direction, respectively, in the first quadrant or the third quadrant, as shown in Fig. 8

$$\begin{cases} \gamma_1 > 0, 1+\beta = \dfrac{\gamma_1}{k_{\mathrm{set}}} > 0: \ \theta_{Z_{\mathrm{cm1}L1'Zr'}} = 90^\circ \to 45^\circ \\ \gamma_1 < 0, 1+\beta = \dfrac{\gamma_1}{k_{\mathrm{set}}} < 0: \ \theta_{Z_{\mathrm{cm1}L1'Zr'}} = -90^\circ \to -135^\circ \end{cases}.$$

Then, the phase angle of $\zeta = I_{\mathrm{cm2}}/I_{L1}$ is discussed in four cases.

1) $1+\beta = -\gamma_1/k_{\mathrm{set}}$, $\gamma_1 > 0$ When k varies from 0 to k_{set}, $\theta_{Z_{\mathrm{cm1}L1'Zr'}} = 90^\circ \to 135^\circ$. In order to change $\theta_{Z\mathrm{in}} = 90^\circ \to 0^\circ$, $\theta_\zeta = 0^\circ \to 135^\circ$ is required. Note that the real part of ζ does not vary with k, only imaginary part changes with k. It is unable to meet the requirement.
2) $1+\beta = -\gamma_1/k_{\mathrm{set}}$, $\gamma_1 < 0$ When k varies from 0 to k_{set}, $\theta_{Z_{\mathrm{cm1}L1'Zr'}} = -90^\circ \to -45^\circ$. In order to change $\theta_{Z\mathrm{in}} = 90^\circ \to 0^\circ$, $\theta_\zeta = -180^\circ \sim -45^\circ$ is required. Obviously, it is also unable to meet the requirement as above.
3) $1+\beta = \gamma_1/k_{\mathrm{set}}$, $\gamma_1 > 0$ When k varies from 0 to k_{set}, $\theta_{Z_{\mathrm{cm1}L1'Zr'}} = 90^\circ \to 45^\circ$. In order to change $\theta_{Z\mathrm{in}} = 90^\circ \to 0^\circ$, $\theta_\zeta = 0^\circ \sim 45^\circ$ is required, which means that the real part > 0, the imaginary part > 0. Thus, the requirement is that $\kappa < \gamma_1 < k_{\mathrm{set}}$ or $\kappa > \gamma_1 > k_{\mathrm{set}}$.
4) $1+\beta = \gamma_1/k_{\mathrm{set}}$, $\gamma_1 < 0$ When k varies from 0 to k_{set}, $\theta_{Z_{\mathrm{cm1}L1'Zr'}} = -90^\circ \to -135^\circ$. In order to change $\theta_{Z\mathrm{in}} = 90^\circ \to 0^\circ$, $\theta_\zeta = -180^\circ \sim -135^\circ$ is required, which means that the real part < 0, the image part < 0. Thus, the requirement is that $\kappa < \gamma_1 < 0$.

In summary, the necessary condition to meet the requirement of the soft switching is:

$$1+\beta = \gamma_1/k_{\mathrm{set}}, \kappa > \gamma_1 > k_{\mathrm{set}} \text{ or } \kappa < \gamma_1 < k_{\mathrm{set}}. \tag{23}$$

V. Design Example and Experimental Validation

In order to validate the proposed design method of compensation network, a WPT prototype based on the T-type compensation network is built.

The input dc voltage U_{d1} is 250 V, and the rated transmission power is 400 W. The circuit is shown in Fig. 9(a), where the primary inverter bridge operates at fixed frequency $f =$ 200 kHz, generating square voltage wave u_{ab}. It should be noted that the frequency does not influence the power transmission characteristic of the compensation network as long as the compensation coefficients remain consistent. According to the latest SAE J2954 Task Force, the frequency of WPT for light duty vehicles centers at 85 kHz. However, the design of power coils is for the demonstration prototype of DWPT with low power. Under the premise that operating frequency is not the key parameter to the design of compensation network, we still use operating frequency 200 kHz for verification. The design of high-power practical wireless charging device in future will choose the 85 kHz. The primary side has a T-type compensation network which is tolerant to large misalignment. If the Z_{cm1} and Z_{cm2} are capacitive, then the *LC* series filter resonating at frequency *f* is needed to be inserted between the inverter and primary compensation network. The capacitor of this filter can be combined with the first capacitive compensation element. The secondary side is a fully compensated S-type network. The high-frequency current in the receiving coil is rectified by the

TABLE I
PARAMETERS OF POWER COILS AND SWITCHES

Component	Parameter
Transmitter coil	$L_1 = 94\ \mu$H, size: 60 cm × 20 cm, $N_1 = 10$
Receiving coil	$L_2 = 91\ \mu$H, size: 20 cm × 30 cm, $N_2 = 12$
The effective range of k	$k = 0.245$–0.12
The requirement of misalignment	The output power fluctuation $<20\%$ in 50% lateral misalignment percentage
Primary MOSFET	IXFH44N50P
Rectifier diode	DSEP 30-06A

noncontrolled rectifier, sending to the dc rated resistance load (R_{d2}) or constant voltage (U_{d2}) load.

The experimental power coils are 5 : 1 physical scale-down models according to the actual sizes of EV and roadway. They are made of *Litz* wires embedded on both sides of the perspex plates and the turns of winding are respectively 10 and 12. To increase the varied range of k for validation of the proposed compensation network, the receiver coil covers with three ferrite magnetic stripes and the vertical gap between transceiver coils becomes 2 cm. The specific sizes of power coils are shown in Fig. 9(b). The parameter of transceiver coils and switches using in the circuit are listed in Table I. The misalignment percentage δ is defined as the ratio of the lateral misalignment Δy to the lateral width of the transmitter coil. The measured k varies with δ is given in Fig. 10(a). When the misalignment percentage is up to 50%, k decreases from 0.245 to 0.115, approximately varying two times ($\alpha \approx 2$). The corresponding measured parameters of the traditional transformer model about transceiver coils are shown in Fig. 10(b). The magnetizing inductance L_m decreases and the leakage inductances L_{l1}, L_{l2} increases when the coupling coefficient k gets small. Whether in the mutual inductance coupling model or the traditional transformer model, the secondary impact on the primary side can both be equivalent to the reflected impedance Z_r. The detailed equivalence has been given in the Appendix A. It should be noted that the theory of compensation network is independent from the design of power coils. The design method of compensation network is not limited in the premise of predesigned power coils. It can be incorporated in the design procedure of power coils as well.

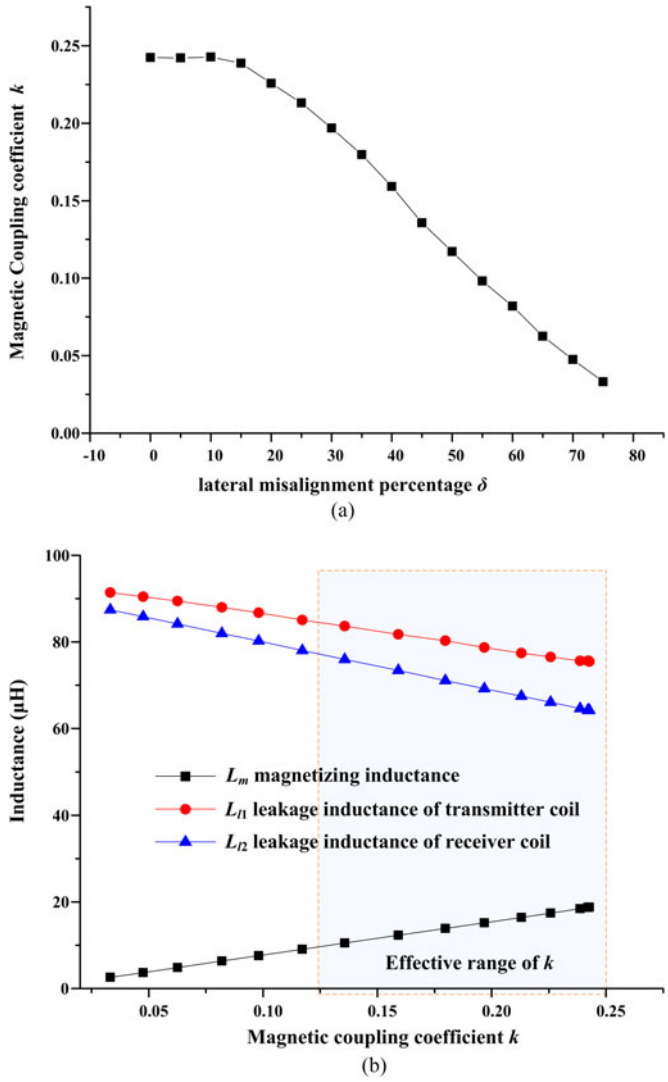

Fig. 10. Measured parameters of transceiver coils at different misalignment. (a) Measured k versus the lateral misalignment percentage Δ. (b) Leakage inductances and magnetizing inductance measured at various k.

A. Design Procedure

According to the previous design optimization in Section IV, the basic design process of the primary T-type compensation network is listed below.

1) Depending on the effective range (0.125, 0.25) of k, the selected coupling point is $k_{\rm set} = \sqrt{\alpha} k_{\rm min} = 0.177$.
2) According to the optimal principle (16) of the transmission efficiency, the secondary optimal quality factor is determined $Q_{\rm load}^{\rm opt} = 1/k_{\rm set} = 5.65$. Then, the equivalent ac load is $R_{\rm ac} = |Z_{L_2}|/Q_{\rm load}^{\rm eff} = 20.22\ \Omega$, and the actual rated dc load is $R_{d2} = R_{\rm ac}/(2\sqrt{2}/\pi)^2 = 25\ \Omega$.
3) Considering the power fluctuation percentage in effective range of k and the transmission power capacity (19) at $k_{\rm set}$, the compensation coefficient γ_1 is selected $|\gamma_1| = 0.29$. Thus, the power curve of compensation network versus k has been identified.
4) According to ZVS soft-switching requirement of the inverter bridge, the compensation coefficient κ is selected. Since $|\gamma_1| = 0.29 > k_{\rm set}$, $\gamma_1 = 0.29$ is selected, meeting the necessary condition (23). Thus, the ratio $\beta = 0.642$. Next, the tendency of $\theta_{Z\rm in}$ with κ at selected point $k_{\rm set}$ is investigated. As shown in Fig. 11(a), the second compensation coefficient is selected $\kappa = 0.7$. The input impedance $Z_{\rm in}$ is slightly inductive at $k_{\rm max}$ and becomes more inductive with larger misalignment as shown in Fig. 11(b). Therefore, the resulting compensation coefficients and compensation elements are selected as follows:

$$\begin{cases} k_{\rm set} = 0.177 \\ \gamma_1 = 0.29 \\ \beta = 0.642 \\ \kappa = 0.7 \end{cases} \Rightarrow \begin{cases} Z_{\rm cm1} = [\gamma_1 - (1+\beta)\kappa]\, Z_{L1} \\ Z_{\rm cm2} = \dfrac{1}{\beta} Z_{\rm cm1} \\ Z_{\rm cm3} = (\kappa - 1) Z_{L1} \end{cases}. \quad (24)$$

The designed T-type compensation network is *CCC* T-type, as shown in Fig. 12. According to the above design parameters, the

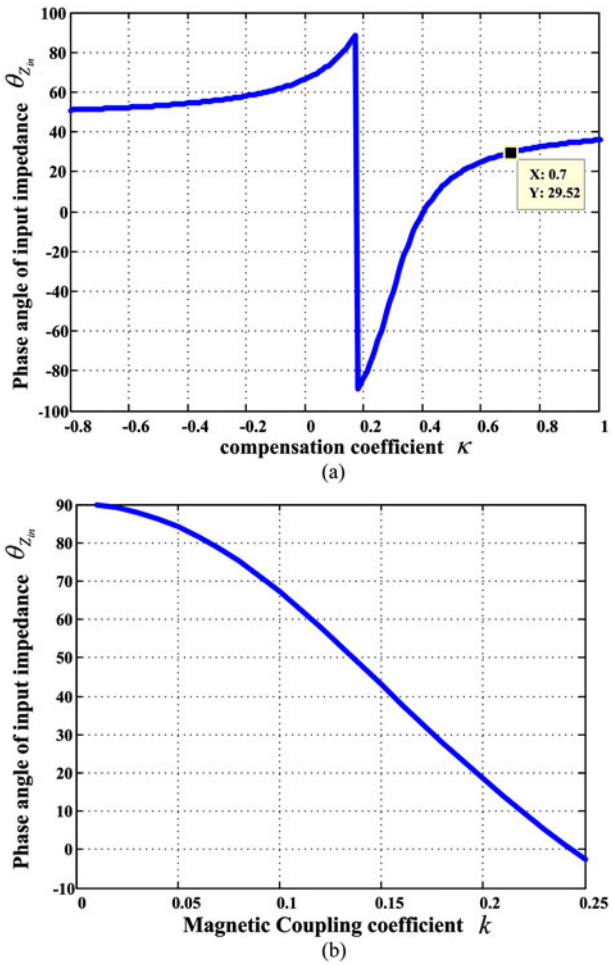

Fig. 11. Phase angle θ_{zin} of input impedance. (a) θ_{zin} varied with κ at $k_{\rm set}$. (b) θ_{zin} varied with k, select $\kappa = 0.7$.

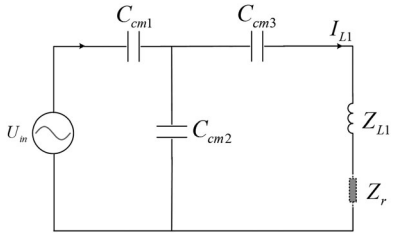

Fig. 12. *CCC* T-type primary compensation network.

primary T-type compensation network is built. The parameters are listed in Table II.

B. Experimental Validation With Rated Resistance Load

To validate the effect of the designed compensation network, the experiment with rated resistance load is carried out. The resistance load $R_{d2} = 25\ \Omega$ is composed of four parallel 100-Ω power resistors. The receiving coil is moved laterally step by step, the currents in each branch and output voltage are recorded at the same time.

Fig. 13 shows the output power versus the coupling coefficient k. The tendency of the experimental result is similar to

TABLE II
PARAMETERS OF THREE-ELEMENT COMPENSATION NETWORK

parameter	Theoretical value	Experimental value
First element	$C_{\rm cm1} = 7.85$ nF	8.05 nF
Second element	$C_{\rm cm2} = 5.03\ \mu$F	4.94 nF
Third element	$C_{\rm cm3} = 22.46$ nF	22.65 nF
γ_1	0.29	0.294
β	0.642	0.617
κ	0.7	0.703

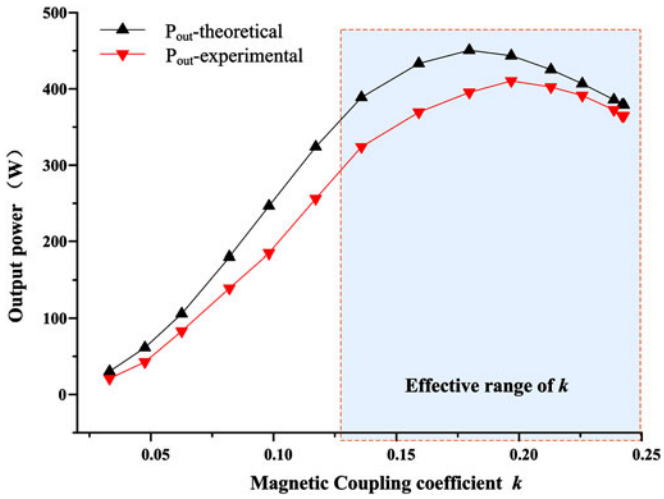

Fig. 13. Output power versus the magnetic coupling coefficient k.

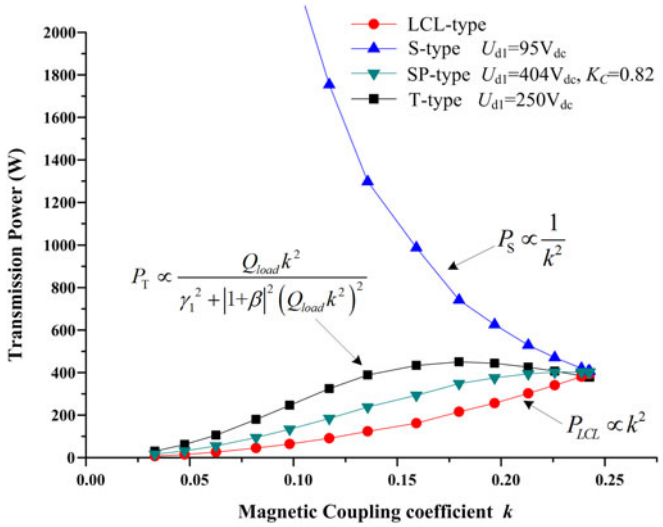

Fig. 14. Transmission power of three types compensation networks versus the coupling coefficient k.

the theoretical curve, whereas some small deviations exist especially at $k_{\rm set}$ point. There are mainly two reasons for the deviations. First, the theoretical model does not take into account the parasitic loss. As can be seen from Fig. 15, the percentage of power loss at the extreme point is about 8%. Second, the maximum transmission power and the actual $k_{\rm set}$ at the extreme point are sensitive to the drift in the parameters of power coils and compensation elements. The detailed sensitivity analysis of the

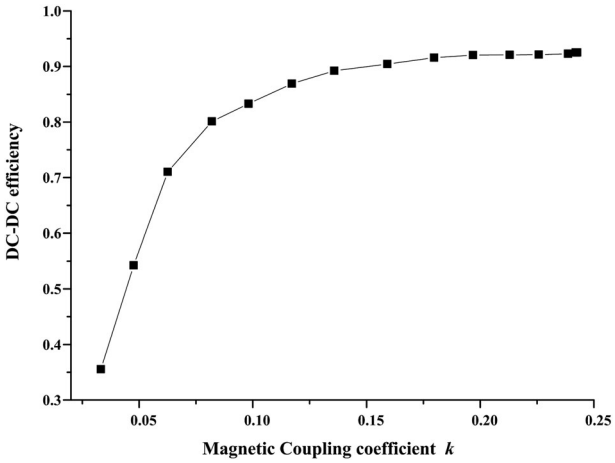

Fig. 15. DC–DC transmission efficiency versus the coupling coefficient k.

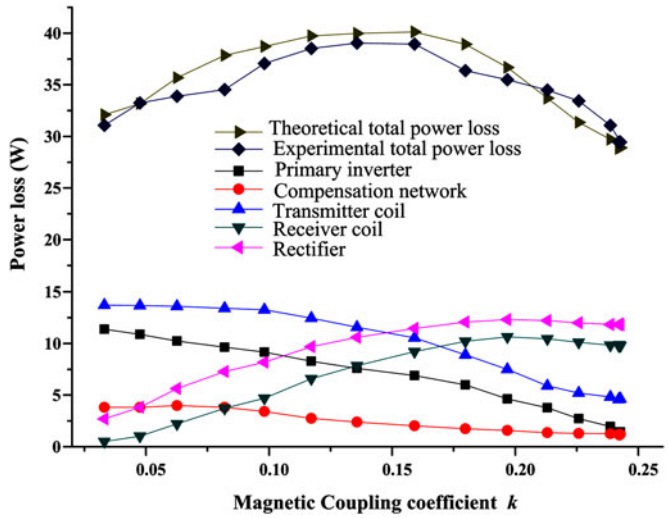

Fig. 16. Total power loss and its calculated distribution at different coupling coefficient k.

proposed DWPT system has been analyzed in the Appendix B. It is found that the system is more sensitive to the detuning of the secondary side and power coils than the drift of the T-type compensation network. Since the theoretical curve in Fig. 13 is calculated from the measured compensation coefficients of T-type compensation network listed in Table II, the influence of the T-type compensation elements has been eliminated. The variation of self-inductances of power coils is less than 0.5%. So the influence of power coils is slight. The premise of theory model in Section III is that the secondary is fully compensated. However, the actual secondary compensation network in experiment has the capacitive deviation percentage $\Delta_2 \approx -1.2\%$, resulting in the slight increase of $\mathrm{k_{set}}$ and the obvious descent of maximum transmission power by 6.8%. Therefore, the total deviation percentage at the extreme point is about 15%. To achieve the designed effect, the secondary compensation network should be kept in tuning state, namely the unity power factor pickup mode.

The comparison of typical primary compensation networks is listed in Table III. The corresponding transmission power characteristics are theoretically studied in Fig. 14. The comparison is carried out under the premise that all compensation networks with the same transceiver power coils and optimal load hold the same transmission power at the $k_{\max}$. So the required input dc voltage U_{d1} is different according to the compensation network type. The *LCL*-type compensation network [25]–[28], which maintains primary coil current constant in spite of k and load, is the one popular type used in DWPT. It can be considered as current excitation type with no compensation elements involved in the self-regulation of transmission power. Its transmission power is reduced in proportion to k^2 when misalignment occurs. The S-type fully compensated network [20], [24], [27], which is the simplest structure, is another popular type used in DWPT. Conversely, the transmission power is greatly increasing in proportion to $1/k^2$ when misalignment occurs. Therefore, it is unsafe without close-loop control when misalignment becomes larger. The SP-type compensation network possesses relative high misalignment tolerance when the suitable factor K_C is chosen [30]. However, the regulation degree is limited compared with the proposed T-type compensation network which has the three design degrees. The transmission power capacity becomes low because the corresponding compensation coefficient γ_1 which has already been determined by the factor K_C is relatively large. According to (19), the required input dc voltage U_{d1} is highest in the four types. Compared to the SP-type, the proposed T-type added only one more compensation element that has three design degrees (γ_1, κ, β) for adjusting the transmission characteristic. With the elaborate design process in Section V-A, the effective range of k maintaining stable power increases two times in the case of no close-loop control. The required input dc voltage U_{d1} can be designed to the desired value even if the rated power capacity and the power coils are first fixed. The transmission power capacity is between the S-type and the SP-type.

As shown in Fig. 15, high dc–dc efficiency over 90% is maintained in the range of k from 0.25 to 0.12. The total power loss and its calculated distribution varied with coupling coefficient k are depicted in Fig. 16. The power loss of the WPT system mainly consists of following parts: the turn-off loss and conduction loss of the primary inverter, T-type compensation network, transmitter coil, receiver coil, and rectifier

$$\begin{aligned} P_{\mathrm{loss}} &= P_{\mathrm{inverter}} + P_{\mathrm{compensation}} + P_{\mathrm{transmitter}} + P_{\mathrm{receiver}} \\ &\quad + P_{\mathrm{rectifier}} \\ &= \left[U_{d1} i_{\mathrm{turn}} (t_r + t_f) f + 2 r_{\mathrm{ds}} I_{\mathrm{cm1}}^2\right] \\ &\quad + \left[r_{\mathrm{cm1}} I_{\mathrm{cm1}}^2 + r_{\mathrm{cm2}} I_{\mathrm{cm2}}^2 + r_{\mathrm{cm3}} I_{L1}^2\right] \\ &\quad + r_{L1} I_{L1}^2 + r_{L2} I_{L2}^2 + 2 u_F I_{L2} \end{aligned} \tag{25}$$

where U_{d1} is the primary input dc voltage, i_{turn} is the current of the MOS switch at the turn-off moment which is increasing as the k becomes small, $(t_r + t_f) \approx 50$ ns is the rise and fall time of the MOS switch, $r_{\mathrm{ds}} \approx 140\ \mathrm{m\Omega}$ is the drain–source on-state resistance of the MOS switch, $r_{\mathrm{cm1}} \approx 480\ \mathrm{m\Omega}$ is the parasitic resistance of filter, the parasitic resistance of other compensation capacitors are less than 50 mΩ, $r_{L1} \approx 460\ \mathrm{m\Omega}$ is the parasitic resistance of the transmitter coil branch, $r_{L2} \approx 550\ \mathrm{m\Omega}$ is the parasitic resistance of the receiver coil branch, and $u_F \approx 1.4$ V

TABLE III
PRIMARY COMPENSATION NETWORKS COMPARISON

Type	Compensation order**	Compensation coefficients	Advantage	Disadvantage	Ref.
LCL	Constant current No elements	–	Constant current in transmission coil	Low misalignment tolerance	[25]–[28]
S*	Voltage excitation One element	κ	Simple structure; Large transmission power capacity	Low misalignment tolerance	[20]
SP*	Voltage excitation Two elements	β, γ_1	Relative high misalignment tolerance	Low transmission power capacity Limited design degree	[30]
T	Voltage excitation Three elements	κ, β, γ_1	High misalignment tolerance; three design degree; lower current stress	Complex structure; Three compensation elements	[This work]

* The "S" mean series, "P" means parallel.
** The compensation order means the number of compensation elements involved in self-regulation of transmission power.

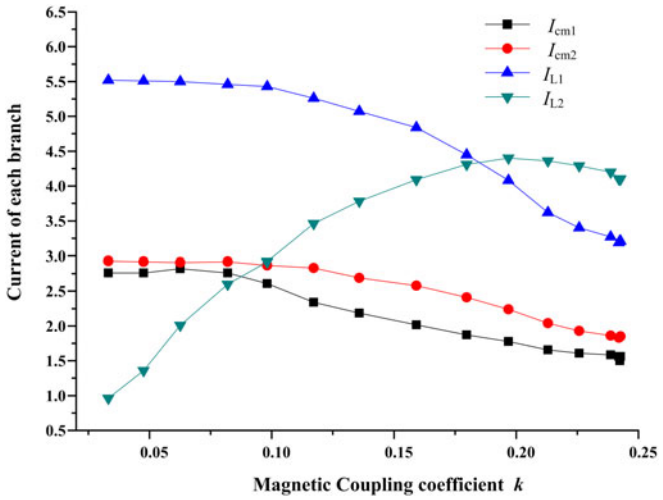

Fig. 17. Each branch current versus the coupling coefficient *k*.

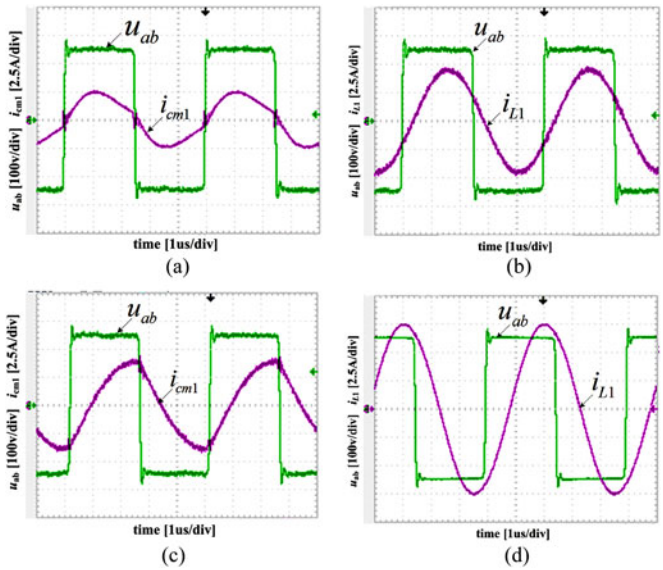

Fig. 18. Output current $i_{\mathrm{cm}1}$, the primary coil current i_{L1}, and square voltage u_{ab} wave of the inverter bridge at different misalignment. (a) Δ is 0%. (b) Δ is 0%. (c) Δ is 50%. (d) Δ is 50%.

is the forward voltage drop of diode in the rectifier. The parasitic resistances are obtained from the measurement by an *LCR* meter and FEM simulation, and the parameters of switch are acquired from datasheet. The u_F is so large that the rectifier loss is always great. Since the input current $I_{\mathrm{cm}1}$ and branch current $I_{\mathrm{cm}2}$ are much smaller than the coil current I_{L1} as shown in Fig. 17, the power loss of compensation network is relatively small. In the range of *k* from 0.25 to 0.12, due to the ZVS state and the low i_{turn} of primary inverter as shown in Fig. 18, the loss of primary inverter is small compared with the main loss resulted from the power coils and rectifier. However, the transmitter coil current I_{L1} and i_{turn} increase greatly when the *k* is less than 0.1, the power loss of transmitter and primary inverter becomes larger. In fact, this range of *k* is out of the effective coupling area and the system should stop the power transmission.

Each branch current versus *k* is shown in Fig. 17. With increasing misalignment between the transceiver coils (*k* deceases), the primary branch current I_{L1} gradually increases, while the secondary current I_{L2} decreases. This tendency of the currents is the instinctive response about the ability of the primary compensation network to automatically regulate the transmission power with varied *k*. When the misalignment increases, the *k* decreases, the reflected impedance Z_r of the secondary side is reduced, and therefore, it needs to increase primary current I_{L1} to maintain the constant transmission power. When the *k* is reduced to zero, namely the receiver coil is completely out of the transmitter coil, the primary branch current increases to a certain value, without any significant overshoot problem, and, therefore, has no-load current limiting capability, which is important for dynamic wireless charging. In addition, the currents in the branch $Z_{\mathrm{cm}1}$ and the branch $Z_{\mathrm{cm}2}$ are approximately the half of the transmitter coil I_{L1}. The power capacity is determined by the maximum currents that the winding of power coils can hold. Therefore, the current stress of the compensation element is relatively small although the T-type has multiple elements.

When the receiving coil is mostly directed above on the transmitter coil ($k = 0.245$), as shown in Fig. 18(a), the output current $i_{\mathrm{cm}1}$ of the inverter bridge slightly lags to the square wave of output voltage u_{ab}, the current in MOSFET switch is small at switching moment and the lag phase angle is close to zero, as slightly inductive. When the misalignment increases to the maximum misalignment percentage $50\%(k = 0.12)$, the

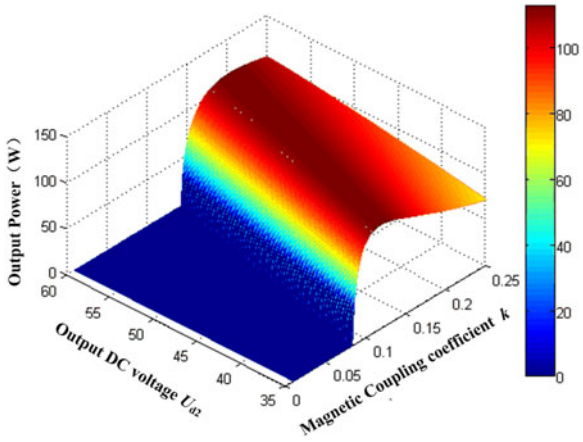

Fig. 19. Theoretical 3-D plot of $P_{\rm out}$ versus U_{d2} and k.

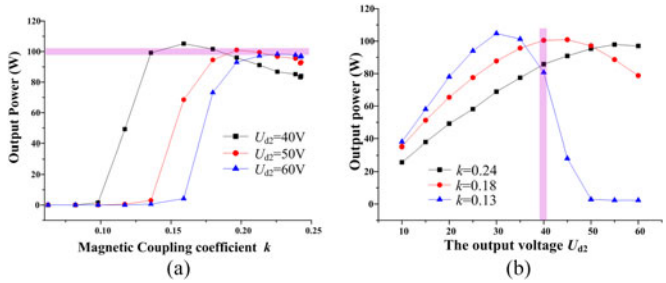

Fig. 20. Experimental output power with constant voltage load. (a) $P_{\rm out}$ versus k under different U_{d2}. (b) $P_{\rm out}$ versus U_{d2} under different k.

lagging phase angle becomes larger, being close to 90°, as shown in Fig. 18(c). During the movement process from $k_{\rm max}$ to 0, the inverter bridge always operates at the soft-switching state which is consistent with the theoretical analysis. Due to the filtering effect of compensation network, the currents in transceiver coils are nearly sinusoidal as shown in Fig. 18(b), (d), reducing the high harmonic frequency (MHz) radiation.

C. Experimental Validation With Constant Voltage Load

According to the design method under the premise of rated resistance load, the resulting T-type compensation network is also suitable for DWPT with constant voltage load. It can keep the transmission power stable even though the coupling coefficient k changes twice. We adopt the CV mode of electronic load as the constant voltage load in the experiment. Considering the maximum power of electronic load used in this experiment is only 300 W, the input dc voltage deceased by half. $U_{d1} = 125$ V and the rated transmission power reduces to 100 W. The output dc current I_{d2} with fixed output dc voltage U_{d2} can be calculated by (15). The theoretical transmission power varied with k at different settled U_{d2} is shown in Fig. 19.

Fig. 20(a) shows the experimental transmission power versus coupling coefficient k at different settled CV mode of electronic load. When the $U_{d2} = 40$ V, the transmission power fluctuation is below 20% in the effective range (0.125, 0.25) of k. Though the effective charging range of k is becoming smaller with increased U_{d2}, the transmission power in effective range k also keeps

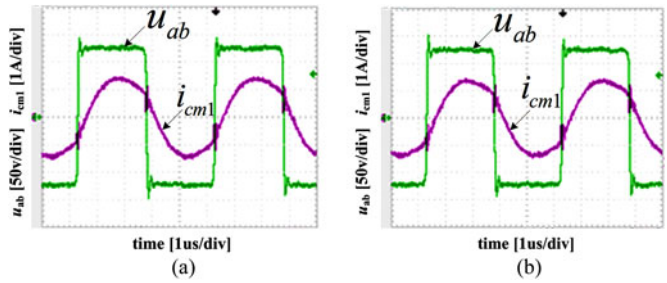

Fig. 21. Output current $i_{\rm cm1}$, and square voltage $u_{\rm ab}$ wave of the inverter bridge at maximum power point under different U_{d2}. (a) $U_{d2} = 40$V, $k = 0.16(\Delta = 40\%)$. (b) $U_{d2} = 60$V, $k = 0.226(\Delta = 20\%)$.

around 100 W with small fluctuation regardless of settled U_{d2}, showing the good ability of maintaining stable power. Furthermore, the transmission power automatically drops to zero when out of effective range of k, avoiding inefficient transmission. The stable transmission power with constant voltage load means that the value of equivalent load keeps almost constant. Thus, the good self-regulation ability of maintaining stable power has been derived from the proposed T-type compensation network designed in Section V-A. When the rated transmission power is maintained, the value of equivalent load is varied according to the settled U_{d2}. As a result, the extreme point k corresponding to the maximum power is deviated from the rated point $k_{\rm set}$ and the effective range of k becomes small when the U_{d2} increases, as shown in Fig. 20(a). Fig. 20(b) shows the experimental transmission power versus the U_{d2} at the settled coupling coefficient k. it can be found that when $k = 0.18$, the transmission power is relatively flat even though the U_{d2} is fluctuated around the extreme point. So the system has the tolerance to output voltage with the slight fluctuation. To pursue the more stable power transmission, the dc–dc converter which regulates the rectifier voltage U_{d2} according to the varied k as well as the output voltage could be considered at the secondary side. The current $i_{\rm cm1}$ of inverter is always lagging to the output voltage $u_{\rm ab}$ as shown in Fig. 21 at maximum power point under different settled U_{d2}. During the movement process from $k_{\rm max}$ to 0, the inverter bridge always operates at the soft-switching state. As a result, the designed compensation network can automatically maintain and regulate the transmission power by itself without the need of complex control on secondary side, making the control of DWPT system simple.

VI. Conclusion

The requirement of DWPT which is different from stationary WPT is analyzed. Since the transmission power of DWPT easily fluctuates over large misalignment, a general design method of primary compensation network is proposed in this paper. The fundamental compensation network based on single compensation element and high-order compensation network consisting of multiple compensation elements are all included in the design method. The power transmission factor is introduced to uniformly describe the transmission characteristics of the primary compensation network. Under the premise of ensuring high transmission efficiency and soft switching, the designed compensation network can maintain a stable output

characteristic over large misalignment; also, a current limiting protection under no-load operation is obtained. At last, a 400-W WPT prototype with a fixed frequency operation based on the T-type there-element compensation network is built. The output power keeps stable within the 200% of the coupling coefficient under constant voltage load or rated resistance load showing the effectiveness of the design method. In the further research, the regulation of dc–dc converter will be added at the secondary side to resist the battery voltage fluctuation and to pursue more stable transmission power in movement.

APPENDIX

A. Comparison Between the Traditional Transformer Model and the Mutual Inductance Coupling Model

There are two theoretical models about coupling power coils. Fig. 22(a) is the mutual inductance coupling model which is adopted in this paper, where L_1, L_2 are, respectively, the self-inductances of transceiver coils, and $M = k\sqrt{L_1 L_2}$ is the mutual inductance. The traditional transformer model is shown in Fig. 22(b), where L_{l1}, L_{l2} are, respectively, the leakage inductances of primary and secondary coils, and L_m is the magnetizing inductance. The turn ratio between both sides is $N = N_1/N_2$.

According to the general circuit theory, the relationship between two models is

$$\begin{cases} L_m = NM = (N_1/N_2)\, M \\ L_{l1} = L_1 - L_m = L_1 - NM \\ L_{l2} = L_2 - L_m/N^2 = L_2 - M/N. \end{cases} \tag{A1}$$

WPT system based on traditional transformer model is shown in Fig. 23. The secondary impact on the primary side is analyzed using the traditional transformer model as following. Since the secondary compensation capacitor is fully compensated with the self-inductance of secondary coil, the reactance of C_2 is

$$Z_{C2} = -j\omega L_2 = -j\omega \left(L_{l2} + L_m/N^2\right). \tag{A2}$$

The impedance of secondary side is

$$Z_{\rm sec} = Z_{C2} + Z_{l2} + R_{\rm ac} = -j\omega L_m/N^2 + R_{\rm ac}. \tag{A3}$$

The secondary side is equivalently converted to the primary side as shown in Fig. 24(a). The equivalent impedance seen from the input port of primary power coil is

$$\begin{aligned} Z_1 &= j\omega L_{l1} + \frac{j\omega L_m \left(-j\omega L_m + N^2 R_{\rm ac}\right)}{j\omega L_m + \left(-j\omega L_m + N^2 R_{\rm ac}\right)} \\ &= j\omega L_{l1} + j\omega L_m + \frac{(\omega L_m)^2}{N^2 R_{\rm ac}} \\ &= j\omega L_1 + \frac{(\omega M)^2}{R_{\rm ac}}. \end{aligned} \tag{A4}$$

The equivalent circuit in Fig. 24(b) is the same as the circuit in Fig. 4(c). Although the leakage inductances and the magnetizing inductance are varied with coupling coefficient k, the self-inductances of transceiver coils are almost fixed, resulting in that the compensation coefficients and transmission power characteristic of the proposed T-type compensation network are unchanged. Therefore, the secondary impact on the primary side can always be represented by the reflected impedance $Z_r = (\omega L_m)^2/(N^2 R_{\rm ac}) = (\omega M)^2/R_{\rm ac}$. From the perspective of the reflected impedance, the self-regulation principle of T-type compensation using the traditional transformer model is the same as the conclusion from the mutual inductance coupling model described in Section III. The current I_{L1} in the transmitter coil also can be described as (6). The current I_2', as shown in Fig. 24(a), is proportional to the secondary coil current $I_{R_{\rm ac}}$, indicating the load component of the primary coil current I_{L1} which transmits the active power to the secondary side

$$I_2' = I_{L1} \frac{(j\omega L_m)}{j\omega L_m + \left(-j\omega L_m + N^2 R_{\rm ac}\right)} = I_{L1} \frac{j\omega M}{N R_{\rm ac}}. \tag{A5}$$

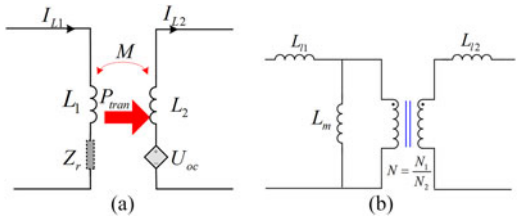

Fig. 22. Two theoretical models of coupling power coils. (a) Mutual inductance coupling model. (b) Traditional transformer model.

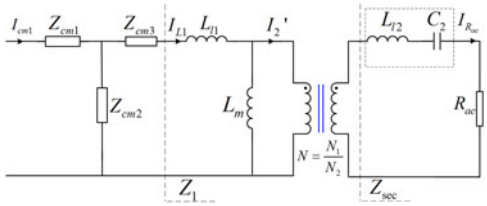

Fig. 23. WPT system based on traditional transformer model.

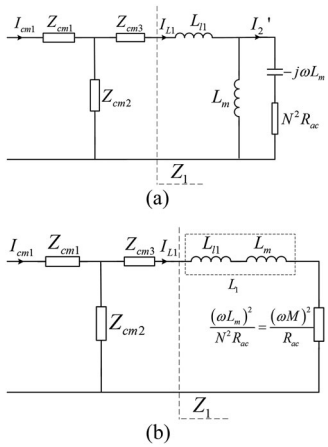

Fig. 24. Equivalent transformation of traditional transformer model. (a) Equivalent transformation of secondary side to primary side. (b) Equivalent transformation of impedance Z_1.

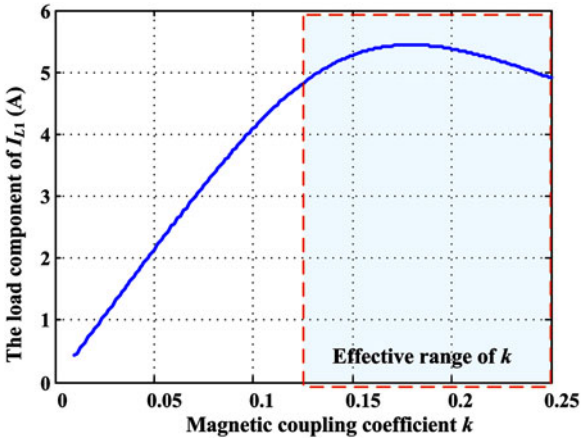

Fig. 25. Load component of I_{L1} versus the coupling coefficient k.

Substituting (6) and (7) into (A5), the current I_2' becomes

$$\begin{aligned} I_2' &= \frac{U_{\text{in}}}{Z_{\text{cm1}} + (\kappa Z_{L1} + Z_r)(1+\beta)} \frac{j\omega M}{N R_{\text{ac}}} \\ &= \frac{U_{\text{in}}}{\gamma_1 Z_{L1} + Z_r(1+\beta)} \frac{j\omega M}{N R_{\text{ac}}} \\ &= \frac{j\omega\sqrt{L_1 L_2}}{N R_{\text{ac}} |Z_{L1}|} \frac{U_{\text{in}}}{\left[\frac{j\gamma_1}{k} + (1+\beta) Q_{\text{load}} k\right]}. \end{aligned} \tag{A6}$$

From the perspective of the traditional transformer model, the load component of the primary-side current is smooth in the vicinity of k_{set} under the self-regulation of the proposed T-type compensation network, as shown in Fig. 25. Therefore, the transmission power is relatively flat in the effective coupling area.

B. Sensitivity Analysis of the Proposed WPT System

1) Influence of the Secondary Detuning: The secondary compensation network possibly has slight detuning in the actual situation. Assuming Δ_2 stands for the percentage of the secondary detuning. The impedance of the secondary circuit is

$$Z_2 = j\omega L_2 + 1/j\omega C_2 + R_{\text{ac}} = (j\Delta_2 + 1/Q_{\text{load}})\,|Z_{L2}|\,. \tag{B1}$$

Substituting (B1) into (2), the reflected impedance is obtained

$$\begin{aligned} Z_r &= \frac{(\omega M)^2}{Z_2} = \frac{(\omega M)^2}{(j\Delta_2 + 1/Q_{\text{load}})\,|Z_{L2}|} \\ &= \frac{-j\Delta_2\,(\omega M)^2}{(\Delta_2^2 + 1/Q_{\text{load}}^2)\,|Z_{L2}|} + \frac{(\omega M)^2}{(\Delta_2^2 + 1/Q_{\text{load}}^2)\,|Z_{L2}|} \frac{1}{Q_{\text{load}}}. \end{aligned} \tag{B2}$$

Generally, the detuning degree is quite tiny, namely $\Delta_2|Z_{L2}| \ll R_{\text{ac}}$, the approximation condition is

$$\Delta_2 \ll 1/Q_{\text{load}}. \tag{B3}$$

Thus, the reflected impedance can be approximated as

$$\begin{aligned} Z_r &\approx -j\Delta_2 \frac{(\omega M)^2}{(1/Q_{\text{load}}^2)\,|Z_{L2}|} + \frac{(\omega M)^2}{1/Q_{\text{load}}\,|Z_{L2}|} \\ &= (-j\Delta_2 \times Q_{\text{load}} + 1)\, k^2 Q_{\text{load}}\,|Z_{L1}|\,. \end{aligned} \tag{B4}$$

Due to the relationship of the rated Q_{load} and k_{set} as shown in (16) the reflected impedance near the k_{set} point becomes

$$Z_r = -\,j\Delta_2\,|Z_{L1}| + k_{\text{set}}\,|Z_{L1}|\,. \tag{B5}$$

The reactance of Z_r resulted from the secondary detuning may influence the compensation coefficient γ_1

$$\begin{aligned} \gamma_1 &= (Z_{L1}' + Z_{\text{cm1}})/Z_{L1} \\ &= \left[(\kappa Z_{L1} - j\Delta_2\,|Z_{L1}|)\,(1+\beta) + Z_{\text{cm1}}\right]/Z_{L1} \\ &= \gamma_1|_{\text{norm}} - \Delta_2\,(1+\beta) \end{aligned} \tag{B6}$$

where $\gamma_1|_{\text{norm}}$ stands for the normal γ_1 without the secondary detuning. The fluctuation of γ_1 is $-\Delta_2(1+\beta)$.

Substituting (16), (18), and (B6) into (9), the coupling coefficient k at the extreme transmission power point is

$$k_{\text{opt}} = \sqrt{\frac{\gamma_1}{|1+\beta|\,Q_{\text{load}}}} = k_{\text{set}}\sqrt{1 - \frac{\Delta_2}{k_{\text{set}}}}. \tag{B7}$$

Considering the approximation (B3), (B7) can be expanded by the Taylor formula, the first-order approximation is

$$k_{\text{opt}} \approx k_{\text{set}}\left(1 - \frac{1}{2}\frac{\Delta_2}{k_{\text{set}}}\right) = k_{\text{set}} - \frac{\Delta_2}{2}. \tag{B8}$$

The deviation of k_{set} due to the secondary detuning is $-\,\Delta_2/2$. Similarly, the maximum transmission power is influenced by the secondary detuning

$$\begin{aligned} P_{\max}(\gamma_1) &= \frac{|U_{in}|^2}{|1+\beta|\,|Z_{L1}|} \frac{1}{2\,|\gamma_1|} \\ &\approx P_{\max}|_{\text{norm}} \left[1 + \frac{(1+\beta)}{\gamma_1|_{\text{norm}}}\Delta_2\right] \end{aligned} \tag{B9}$$

where $P_{\max}|_{\text{norm}}$ is the normal maximum transmission power without the secondary detuning. The relative fluctuation of the maximum transmission power is

$$\frac{\delta P_{\max}}{P_{\max}|_{\text{norm}}} = \frac{(1+\beta)}{\gamma_1|_{\text{norm}}}\Delta_2 = \frac{\Delta_2}{k_{\text{set}}}. \tag{B10}$$

If the $\Delta_2 = 1\%$, the deviation of k_{set} is 0.005, the fluctuation of $P_{\max}$ is 5.7%.

2) Influence of the Drift in the Transmitter Coil's Self-Inductance: The drift in the transmitter coil's self-inductance can influence the compensation coefficient γ_1, resulting in the fluctuation of extreme point k_{set} and the maximum transmission power. It is similar to the case of the secondary detuning. Assuming Δ_1 is the percentage of the primary self-inductance drift. The self-inductance reactance of transmitter coil is $Z_{L1} = (1+\Delta_1)\,Z_{L1}|_{\text{norm}}$. The maximum transmission power is analyzed as follows:

$$\begin{aligned} P_{\max}(\gamma_1) &= P_{\max}|_{\text{norm}} \frac{1}{(1+\Delta_1)\left[1 + (1+\beta)\,\Delta_1/\,\gamma_1|_{\text{norm}}\right]} \\ &\approx P_{\max}|_{\text{norm}} \frac{1}{\left[1 + (1/k_{\text{set}} + 1)\,\Delta_1\right]} \\ &\approx P_{\max}|_{\text{norm}}\left[1 - (1/k_{\text{set}} + 1)\,\Delta_1\right]. \end{aligned} \tag{B11}$$

Therefore, the relative fluctuation of the maximum transmission power is

$$\frac{\delta P_{\max}}{P_{\max}|_{\text{norm}}} = -\left(\frac{\Delta_1}{k_{\text{set}}} + \Delta_1\right). \tag{B12}$$

The deviation of k_{set} due to the primary self-inductance drift is similar to the case of the secondary detuning

$$k_{\text{opt}} \approx k_{\text{set}} + \frac{\Delta_1}{2}. \tag{B13}$$

Considering the Z_{cm3} is in series with the transmitter coil, the drift in Z_{cm3} is also included in this case. If the $\Delta_1 = 1\%$, the deviation of k_{set} is 0.005, the fluctuation of $P_{\max}$ is 6.6%.

3) Influence of the Drifts in the Primary Compensation Elements: The drifts in Z_{cm1} and Z_{cm2} may influence the compensation coefficient β, resulting in the fluctuation of extreme point k_{set} and the maximum transmission power. Assuming Δ_{cm1} and Δ_{cm1} are, respectively, the percentages of the Z_{cm1} and Z_{cm2} drifts. The fluctuation of $\beta = Z_{\text{cm1}}/Z_{\text{cm2}}$ is

$$\begin{aligned}\delta\beta &= \frac{\partial\beta}{\partial Z_{\text{cm1}}}\delta Z_{\text{cm1}} + \frac{\partial\beta}{\partial Z_{\text{cm2}}}\delta Z_{\text{cm2}} \\ &= \beta|_{\text{norm}}\left(\Delta_{\text{cm1}} - \Delta_{\text{cm2}}\right).\end{aligned} \tag{B14}$$

The compensation coefficient γ_1 is influenced by the $\delta\beta$

$$\gamma_1 = \left[\kappa Z_{L1}(1+\beta) + Z_{\text{cm1}}\right]/Z_{L1} = \gamma_1|_{\text{norm}} + \kappa \times \delta\beta. \tag{B15}$$

The coupling coefficient *k* at the extreme transmission power point is

$$\begin{aligned}k_{\text{opt}} &= \sqrt{\frac{\gamma_1}{|1+\beta|\, Q_{\text{load}}}} \approx \sqrt{\frac{\gamma_1 k_{\text{set}}}{1+\beta|_{\text{norm}}}} + \frac{\partial k_{\text{opt}}}{\partial\beta}\delta\beta \\ &= k_{\text{set}}\left[1 + \frac{1}{2}\left(-\frac{1}{1+\beta|_{\text{norm}}} + \frac{\kappa}{\gamma_1}\right)\delta\beta\right].\end{aligned} \tag{B16}$$

The maximum transmission power at extreme point k_{opt} is

$$\begin{aligned}P_{\max}(\gamma_1) &= \frac{|U_{\text{in}}|^2}{2\,|1+\beta|\,|Z_{L1}|}\frac{1}{|\gamma_1|} \\ &\approx \frac{|U_{\text{in}}|^2}{2\,|Z_{L1}|}\frac{1}{(1+\beta)\,\gamma_1|_{\text{norm}} + [\gamma_1|_{\text{norm}} + (1+\beta)\,\kappa]\,\delta\beta} \\ &= P_{\max}|_{\text{norm}}\left\{1 - \frac{[\gamma_1|_{\text{norm}} + (1+\beta)\,\kappa]}{(1+\beta)\,\gamma_1|_{\text{norm}}}\delta\beta\right\}.\end{aligned} \tag{B17}$$

If the fluctuation of β is less than 1%, the drift of the extreme point k_{opt} is less than 0.86%. The fluctuation of $P_{\max}$ is less than 1.85%. When the suitable values of compensation components are chosen, the variations of these values are quite small with little influence on the fluctuation of the transmission power.

REFERENCES

[1] S. Y. R. Hui and W. W. C. Ho, "A new generation of universal contactless battery charging platform for portable consumer electronic equipment," *IEEE Trans. Power Electron.*, vol. 20, no. 3, pp. 620–627, May 2005.

[2] Q. Chen, S. C. Wong, C. K. Tse, and X. Ruan, "Analysis, design, and control of a transcutaneous power regulator for artificial hearts," *IEEE Trans. Biomed. Circuits Syst.*, vol. 3, no. 1, pp. 23–31, Feb. 2009.

[3] S. Li and C. C. Mi, "Wireless power transfer for electric vehicle applications," *IEEE J. Emerg. Sel. Topics Power Electron.*, vol. 3, no. 1, pp. 4–17, Mar. 2015.

[4] G. A. Covic and J. T. Boys, "Modern trends in inductive power transfer for transportation applications," *IEEE J. Emerg. Sel. Topics Power Electron.*, vol. 1, no. 1, pp. 28–41, Mar. 2013.

[5] S. Y. Choi, B. W. Gu, S. Y. Jeong, and C. T. Rim, "Advances in wireless power transfer systems for roadway-powered electric vehicles," *IEEE J. Emerg. Sel. Topics Power Electron.*, vol. 3, no. 1, pp. 18–36, Mar. 2015.

[6] Systems Control Technology, Inc., "Roadway powered electric vehicle project: Track construction and testing program phase 3D," California PATH Program, Inst. Transportation Studies, Univ. California, Berkeley, CA, USA, Tech. Rep. UCB-ITS-PRR-94-07, 1994.

[7] S. Chopra and P. Bauer, "Driving range extension of EV With on-road contactless power transfer—A case study," *IEEE Trans. Ind. Electron.*, vol. 60, no. 1, pp. 329–338, Jan. 2013.

[8] Y. Zhang, K. Chen, F. He, Z. Zhao, T. Lu, and L. Yuan, "Closed-form oriented modeling and analysis of wireless power transfer system with constant-voltage source and load," *IEEE Trans. Power Electron.*, vol. 31, no. 5, pp. 3472–3481, May 2016.

[9] X. Qu, H. Han, S. –C. Wong, C. K. Tse, and W. Chen, "Hybrid IPT topologies with constant current or constant voltage output for battery charging applications," *IEEE Trans. Power Electron.*, vol. 30, no. 11, pp. 6329–6337, Nov. 2015.

[10] Z. Fang, T. Cai, S. Duan, and C. Chen, "Optimal design methodology for LLC resonant converter in battery charging applications based on time-weighted average efficiency," *IEEE Trans. Power Electron.*, vol. 30, no. 10, pp. 5469–5483, Oct. 2015.

[11] A. Caillierez, D. Sadarnac, A. Jaafari, and S. Loudot, "Dynamic inductive charging for electric vehicle: Modeling and experimental results," in *Proc. 7th IET Int. Conf. Power Electron. Mach. Drives*, 2014, pp. 1–7.

[12] A. Caillierez, D. Sadarnac, A. Jaafari, and S. Loudot, "Unlimited range for electric vehicles," in *Proc. Int. Symp. Power Electron. Electr. Drives Autom. Motion*, 2014, pp. 941–946.

[13] S. Jeong, Y. J. Jang, and D. Kum, "Economic analysis of the dynamic charging electric vehicle," *IEEE Trans. Power Electron.*, vol. 30, no. 11, pp. 6368–6377, Nov. 2015.

[14] V. Prasanth and P. Bauer, "Distributed ipt systems for dynamic powering: Misalignment analysis," *IEEE Trans. Ind. Electron.*, vol. 61, no. 11, pp. 6013–6021, Nov. 2014.

[15] Y. Nagatsuka, S. Noguchi, Y. Kaneko, S. Abe, T. Yasuda, K. Ida, A. Suzuki, and R. Yamanouchi, "Contactless power transfer system for electric vehicle battery charger," in *Proc. 25th World Battery Hybrid Fuel Cell Symp. Exhibit.*, China, 2010, pp. 1–6.

[16] M. Budhia, J. T. Boys, G. A. Covic, and C. Y. Huang, "Development of a single-sided flux magnetic coupler for electric vehicle IPT charging systems," *IEEE Trans. Ind. Electron.*, vol. 60, no. 1, pp. 318–328, Jan. 2013.

[17] S. Y. Choi, J. Huh, W. Y. Lee, and C. T. Rim, "Asymmetric coil sets for wireless stationary EV chargers with large lateral tolerance by dominant field analysis," *IEEE Trans. Power Electron.*, vol. 29, no. 12, pp. 6406–6420, Dec. 2014.

[18] C. Zheng, H. Ma, J. S. Lai, and L. Zhang, "Design considerations to reduce gap variation and misalignment effects for the inductive power transfer system," *IEEE Trans. Power Electron.*, vol. 30, no. 11, pp. 6108–6119, Nov. 2015.

[19] J. Deng, W. Li, T. D. Nguyen, S. Li, and C. C. Mi, "Compact and efficient bipolar coupler for wireless power chargers: Design and analysis," *IEEE Trans. Power Electron.*, vol. 30, no. 11, pp. 6130–6140, Nov. 2015.

[20] J. Huh, S. W. Lee, W. Y. Lee, G. H. Cho, and C. T. Rim, "Narrow-width inductive power transfer system for online electrical vehicles," *IEEE Trans. Power Electron.*, vol. 26, no. 12, pp. 3666–3679, Dec. 2011.

[21] C. Park, S. Lee, S. Y. Jeong, G. H. Cho, and C. T. Rim, "Uniform power I-type inductive power transfer system with DQ-power supply rails for on-line electric vehicles," *IEEE Trans. Power Electron.*, vol. 30, no. 11, pp. 6446–6455, Nov. 2015.

[22] C. S. Wang, O. H. Stielau, and G. A. Covic, "Design considerations for a contactless electric vehicle battery charger," *IEEE Trans. Ind. Electron.*, vol. 52, no. 5, pp. 1308–1314, Oct. 2005.

[23] C. S. Wang, O. H. Stielau, and G. A. Covic, "Load models and their application in the design of loosely coupled inductive power transfer systems," in *Proc. IEEE Int. Conf. Power Syst. Technol.*, 2000, pp. 1053–1058.

[24] W. Zhang and C. Mi, "Compensation topologies for high power wireless power transfer systems," *IEEE Trans. Vehicular Technol.*, to be published, DOI: 110.1109/TVT.2015.2454292, 2015.

[25] M. L. G. Kissin, C. Y. Huang, G. A. Covic, and J. T. Boys, "Detection of the tuned point of a fixed-frequency LCL resonant power supply," *IEEE Trans. Power Electron.*, vol. 24, no. 4, pp. 1140–1143, Apr. 2009.
[26] C. Y. Huang, J. T. Boys, and G. A. Covic, "Resonant network design considerations for variable coupling lumped coil systems," in *Proc. IEEE Energy Convers. Congr. Expo*, 2012, pp. 3841–3847.
[27] B. Esteban, M. Sid-Ahmed, and N. C. Kar, "A comparative study of power supply architectures in wireless EV charging systems," *IEEE Trans. Power Electron.*, vol. 30, no. 11, pp. 6408–6422, Nov. 2015.
[28] H. H. Wu, A. Gilchrist, K. D. Sealy, and D. Bronson, "A high efficiency 5 kW inductive charger for EVs using dual side control," *IEEE Trans. Ind. Informat.*, vol. 8, no. 3, pp. 585–595, Aug. 2012.
[29] J. Hou, Q. Chen, S. C. Wong, C. K. Tse, and X. Ruan, "Analysis and control of series/series-parallel compensated resonant converters for contactless power transfer," *IEEE J. Emerg. Sel. Topics Power Electron.*, vol. 3, no. 1, pp. 124–136, Mar. 2015.
[30] J. L. Villa, J. Sallan, J. F. S. Osorio, and A. Llombart, "High-misalignment tolerant compensation topology for ICPT systems," *IEEE Trans. Ind. Electron.*, vol. 59, no. 2, pp. 945–951, Feb. 2012.
[31] N. A. Keeling, G. A. Covic, and J. T. Boys, "A unity-power-factor IPT pickup for high-power applications," *IEEE Trans. Ind. Electron.*, vol. 57, no. 2, pp. 744–751, Feb. 2010.
[32] Y. Zhang, T. Lu, Z. Zhao, F. He, K. Chen, and L. Yuan, "Selective wireless power transfer to multiple loads using receivers of different resonant frequencies," *IEEE Trans. Power Electron.*, vol. 30, no. 11, pp. 6001–6005, Nov. 2015.
[33] J. Zhao, H. Feng, T. Cai, S. Duan, and Q. Dai, "The complex ratio transformer model and its application in magnetic resonant WPT," in *Proc. IEEE Transportation Electrification Asia-Pacific Conf. Expo.*, Beijing, China, 2014, pp. 1–5.
[34] R. Lu, T. Wang, Y. Mao, and C. Zhu, "Analysis and design of a wireless closed-loop ICPT system working at ZVS mode," in *Proc. IEEE Veh. Power Propul. Conf.*, 2010, pp. 1–5.
[35] W. Zhong, and S. Y. R. Hui, "Maximum energy efficiency tracking for wireless power transfer systems," *IEEE Trans. Power Electron.*, vol. 30, no. 7, pp. 4025–4034, Jul. 2015.
[36] M. Fu, H. Yin, X. Zhu, and C. Ma, "Analysis and tracking of optimal load in wireless power transfer systems," *IEEE Trans. Power Electron.*, vol. 30, no. 7, pp. 3952–3963, Jul. 2015.

Jinbo Zhao received the B.S. and M.S. degrees in theoretical physics from the Huazhong University of Science and Technology, Wuhan, Hubei, China, in 2008 and 2011, respectively, where he is currently working toward the Ph.D. degree at the School of Electrical and Electronics Engineering.

His research interests include wireless power transmission and power electronics applied to electric vehicles.

Tao Cai received the Ph.D. degree in control science and engineering from the Huazhong University of Science and Technology, Wuhan, China, in 2004.

He is currently at the Huazhong University of Science and Technology. He has authored or coauthored more than 20 technical papers in journal and conferences. His current research interests include advanced signal processing and energy management of renewable power generation.

Shanxu Duan (M'14) received the B.S., M.S., and Ph.D. degrees in electrical engineering from the Huazhong University of Science and Technology, Wuhan, China, in 1991, 1994, and 1999, respectively.

Since 1991, he has been a Faculty Member at the College of Electrical and Electronics Engineering, Huazhong University of Science and Technology, where he is currently a Professor. His research interests include stabilization, nonlinear control with application to power electronic circuits and systems, fully digitalized control techniques for power electronics apparatus and systems, and optimal control theory and corresponding application techniques for high-frequency pulse width modulation power converters.

Dr. Duan is a Senior Member of the Chinese Society of Electrical Engineering and a Council Member of the Chinese Power Electronics Society. He was selected as one of the New Century Excellent Talents by the Ministry of Education of China in 2007. He received the honor of "Delta Scholar" in 2009.

Hao Feng received the B.S. degree in automation engineering from the Huazhong University of Science and Technology, Wuhan, China, in 2013, where he is currently working toward the Ph.D. degree at the School of Electrical and Electronics Engineering.

His research interests include inductive power transfer systems, resonant converters and renewable energy applications.

Changsong Chen received the Ph.D. degree in electrical engineering from the Huazhong University of Science and Technology, Wuhan, China, in 2011.

He was a Postdoctoral Research Fellow with the Department of Control Science and Engineering, Huazhong University of Science and Technology, from 2011 to 2013. He is currently a Faculty Member at the School of Electrical and Electronics Engineering, Huazhong University of Science and Technology. His current research interests include renewable energy applications, microgrid, and power electronics applied to electric vehicles.

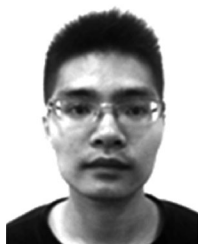

Xiaoming Zhang received the B.S. degree in electrical engineering and automation from the Huazhong University of Science and Technology, Wuhan, China, in 2014, where he is currently working toward the Ph.D. degree at the School of Electrical and Electronics Engineering.

His research interests include wireless power transmission and power electronics applied to electric vehicles.